Cover Page - Example

Bayesian Inference for Geothermal Model Calibration

TIANGANG CUI[1]
Engineering Science, University of Auckland, Auckland, NZ

COLIN FOX[2]
Mathematics, University of Auckland, Auckland, NZ

GEOFF NICHOLLS[3]
Statistics, University of Oxford

MICHAEL O'SULLIVAN[1]
Engineering Science, University of Auckland, Auckland, NZ

Total No of pages (Excluding Cover Page) = 6 (maximum)

Full addresses/phone/fax

[1] Department of Engineering Science, University of Auckland, Private Bag 92019, Auckland 1142, NZ
.
Ph. (64 9) 3737 599 ext 88393 Fax (64 9) 3737 468

[2] Department of Mathematics, University of Auckland, Private Bag 92019, Auckland 1142, NZ

Ph. (64 9) 3737 599 ext. 87316 Fax (64 9) 3737 457

[3] Department of Statistics, University of Oxford, 1 South Parks Road, Oxford, OX1 3TG, U.K.

Ph. (+44) 1865 281224

BAYESIAN INFERENCE FOR GEOTHERMAL MODEL CALIBRATION

TIANGANG CUI[1], COLIN FOX[2], GEOFF NICHOLLS[3] AND MICHAEL O'SULLIVAN[1]

[1] Department of Engineering Science, University of Auckland, Auckland, NZ
[2] Department of Mathematics, University of Auckland, Auckland, NZ
[3] Department of Statistics, University of Oxford, UK

SUMMARY – The aim of this work is the development of a method that will allow the automated calibration of computer models of geothermal fields. The mathematical method used is Markov chain Monte Carlo (MCMC) sampling from the posterior distribution. The technique is applied to calibrating a simple single-layer model of the feed-zone of a well, using discharge test measurements of flowing enthalpy and well-head pressure, and secondly to calibrating a large 3D natural state model using pre-exploitation measurements of temperature versus depth in several wells.

1. INTRODUCTION

The most difficult task in setting up a computer model of a geothermal field is the estimation of parameters such as permeability and porosity. This inverse modelling or calibration process is carried out by matching the model results to field data. Because geothermal systems are highly heterogeneous and anisotropic and field observations are usually sparse, model calibration is difficult and time consuming both in terms of computer time and human input. The present study is part of a major investigation of methods for automating model calibration. It investigates model calibration, or the inverse geothermal modelling problem, as a problem in statistical inference using a Bayesian framework.

Past approaches to the inverse problem of geothermal modelling have used a deterministic approach based on nonlinear optimization methods for calculating 'optimum' parameter values [1]. Some success has been achieved with these methods for simple models with few parameters but they do not work well for large complex models [2]. Also they do not generate information about the likely deviations in predictions made from an optimized model.

Statistical Inference is a well-developed area of Science devoted to drawing conclusions from quantitative measurements that we apply here to geothermal model calibration. Bayesian methods are now well established as a route to quantifying and solving ill-posed inverse problems [3-7], and have a significant advantage over standard least-squares by producing robust estimates along with quantified errors [8]. In a Bayesian formulation, predictions are based on the posterior distribution over *all* solutions consistent with the data, accounting for measurement and modeling uncertainties. Indeed, the posterior density given by Bayes' formula is simply a quantification of the relative probability of a set of parameters being the correct solution, given the measurements and various uncertainties. Robust predictions are then possible as averages of desired quantities, or statistics, over the posterior distribution. We formalize those statements as follows.

Let $\tilde{d}$ and D denote the observed data and data space respectively, and θ and Θ denote the parameter and parameter space respectively. All information pertinent to the model calibration is contained in the unnormalized posterior distribution for $\theta \in \Theta$ conditional on $\tilde{d} \in D$. This is given by Bayes' rule:

$$\pi(\theta|\tilde{d}) \propto L(\tilde{d}|\theta)\pi_{pr}(\theta) \qquad (1)$$

where $L(\tilde{d}|\theta)$ and $\pi_{pr}(\theta)$ are the likelihood function and prior distribution, respectively. Note that the posterior distribution is a density over the (high-dimensional) parameter space Θ and is not useful as a solution in that form. Useful solutions are given by summary statistics of the posterior distribution that can always be written as the posterior expectation of some statistic h, i.e.

$$E_{\pi}[h(\theta)] = \int_{\Theta} h(\theta)\pi(\theta|\tilde{d})d\theta. \qquad (2)$$

The statistic $h(\theta)$ can be any function of the parameter θ in which we are interested. Uncertainties in the posterior expectation of h may be calculated similarly.

The integral required in (2) is over all possible solutions, and represents a sizable computational task. However, such integrals are feasible with the best current technology being the Markov chain Monte Carlo (MCMC) algorithms developed in the field of computational statistics. These approximate (2) via the Monte Carlo quadrature

$$\int_{\Theta} h(\theta)\pi(\theta|\tilde{d})d\theta \approx \frac{1}{N}\sum_{n=1}^{N} h(\theta_n) \qquad (3)$$

where θ_n are samples drawn from the posterior distribution. The approximation converges according to a central limit theorem, with expected variance of the RHS decreasing with increasing N . Our MCMC implementation is outlined in section 5.

Our methodology is applied first to determining the parameters for a simple single-layer model of the feed-zone of a well, using discharge test measurements of flowing enthalpy and well-head pressure, and secondly to calibrating a large 3D natural state model using pre-exploitation measurements of temperature versus depth in several wells.

2. FORWARD PROBLEM

Multiphase non-isothermal flow in a geothermal reservoir is governed by mass the and energy balance equations

$$\frac{d}{dt}\int_{\Omega} M_\alpha dV = \int_{\partial\Omega} Q_\alpha . \hat{n} d\Gamma + \int_{\Omega} q_\alpha dV \qquad (4)$$

The accumulation term M_α represents mass (α=m) or energy (α=e) per unit volume, Q_α represents mass or energy flux, calculated from

$$M_m = \phi(\rho_l S_l + \rho_v S_v)$$
$$M_e = (1-\phi)\rho_r c_r T + \phi(\rho_l u_l S_l + \rho_v u_v S_v)$$
$$Q_{ml} = -\frac{k k_{rl}}{\nu_l}\left[\nabla p - \rho_l \underline{g}\right]$$
$$Q_{mv} = -\frac{k k_{rv}}{\nu_v}\left[\nabla p - \rho_v \underline{g}\right]$$
$$Q_m = Q_{ml} + Q_{mv}$$
$$Q_e = h_l Q_{ml} + h_v Q_{mv} - K\nabla T$$

Here ϕ, k, k_{rl} and k_{rv} are the porosity, permeability and relative permeabilities, respectively. The van Genuchten-Mualem relative permeability model [9] with $S_{rv} = 0$ is adopted in this paper. The mass flow of water and steam are denoted by Q_{ml} and Q_{mv}, respectively.

Equation (4) is discretised with the finite volume method and solved with the numerical simulator TOUGH2 [9]. For the well-discharge problem a 1D radial grid is used whereas for the natural state reservoir model a 3D regular rectangular grid is used, with some mesh refinement in the production zone.

3. BAYESIAN INFERENCE

Figure 1 gives a schematic of the distributions of possible data and recovered parameters when uncertainty in measurement and noise in modelling is considered. A true parameter θ_{true} results in ideal, noise-free data d_{nf} under the forward map (usually a numerical approximation to the real problem). Because of noise in measurements we do not actually measure the data d_{nf}, but rather some noisy version. The range of possible observed data, considering the range of possible corruption by noise, is shown as a shaded region around d_{nf}. In a particular experiment we observe a single data set $\tilde{d}$ and the noise realization is unknown. By using some model-fitting procedures such as manual calibration or nonlinear optimization (with ITOUGH2 for example [1]), we may find θ_{ML} which is typically the maximum likelihood (ML) estimate of the parameter. Because of the noise associated with $\tilde{d}$ and numerical approximation of the forward map, there is in fact a range of feasible parameters each consistent with the measured data up to a feasible noise vector. The shaded region around θ_{ML} shows these.

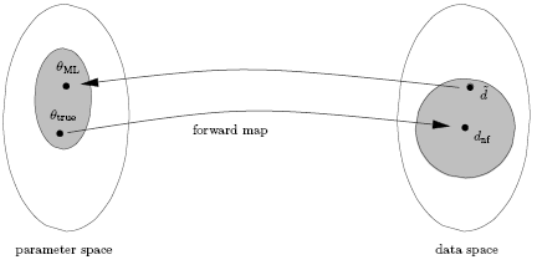

Figure 1. A schematic showing the parameter space, the data space and the forward map.

As discussed in section 1, Bayes' rule quantifies the distribution of feasible parameter values using the details of the forward map and estimates of the measurement noise process. In (1) the likelihood function $L(\tilde{d}|\theta)$ is the probability density function for $\tilde{d}$ given θ, which represents a measure of how likely it is that a parameter θ is true given an observation $\tilde{d}$. In past deterministic optimization techniques for geothermal calibration (e.g. ITOUGH2), the objective function (sum of squares of the differences of the model outputs and observations) can be considered as the logarithm of the likelihood function when Gaussian noise is assumed. The prior $\pi_{pr}(\theta)$ models the state of knowledge about the unknown true value of θ in the absence of measured data $\tilde{d}$. While $\pi_{pr}(\theta)$ reflects the belief about θ prior to experimentation, the posterior $\pi(\theta|\tilde{d})$ reflects the belief about θ after observing $\tilde{d}$. Since $\pi(\theta|\tilde{d})$ represents the probability distribution of θ, Bayesian inference produces information about the distribution of the parameter θ, rather than a single value estimate.

In our study, we assume the observed data has independent and normally distributed

measurement errors with zero mean and variances σ_i^2:

$$\overline{d}_i = d_i + \varepsilon_i, \quad i = 1...N$$

Here d_i is the unknown real parameter value, N is the total number of measurements and $\varepsilon_i \sim N(0, \sigma_i)$. Therefore, the calculation of likelihood is straight forward:

$$L(\tilde{d}|\theta) \propto \prod_{i=1}^{N} \exp\left(-\frac{(\overline{d}_i - d_i^M)^2}{2\sigma_i^2} \right)$$

Construction of the prior density is an important step in performing the statistical inverse problem. Our prior knowledge of the unknown is usually qualitative rather than quantitative. Hence we must transform qualitative information into quantitative probability densities. The prior probability distribution should be concentrated on those values of parameters that an expert expects to see and higher probabilities must be assigned to them rather than to those that are not expected to appear. The details will be discussed in the following sections.

4. MODELLING AND INFERENCE

Forming the posterior distribution in (1) requires two modelling steps that are not often explicitly considered in deterministic approaches. The likelihood function $L(\tilde{d}|\theta)$ is derived as the probability density for measuring data $\tilde{d}$ when the true parameters are θ. What is required is a probabilistic model for measurement errors as well as the deterministic forward map. To clarify these concepts, consider a deterministic forward map $d(\theta)$ with measurements corrupted by additive errors e having probability density function $f(e)$. Then the likelihood function is simply

$$L(\tilde{d}|\theta) = f\left(\tilde{d} - d(\theta)\right) \qquad (5)$$

since the Jacobian determinant for the change of variables from e to $\tilde{d}$ equals 1. The functional form of f is typically determined by modelling the measurement process based on repeated measurements where available, knowledge of the instrumentation, or by analysing an existing data set. In this work we analysed an existing data set, using high frequency structure too infer the scale of intrinsic measurement errors, some detective work to find data that were interpolated rather than measured, and a model for the data dependence between measured points that we validated by numerical simulation. For simplicity we took f to be Gaussian with independent errors where feasible. Errors in the deterministic forward map may also be included in the likelihood function, and can lead to improved inference (see e.g. [7]). We are developing that analysis in an extension of the study presented here.

Secondly, stochastic modelling of the unknown true parameters is required to form the prior distribution $\pi_{pr}(\theta)$. This distribution gives the relative probability for parameters θ in the absence of data. Prior models are typically derived from expert knowledge of allowable parameter values, previous measurements, modelling of processes that produce the unknown parameters, or a combination of these. The representation of unknowns is a composite part of prior modelling since expressing certain types of knowledge is simpler in some representations than others, and solutions that cannot be represented are excluded. In this work we represented the state by the vector of coefficients in a finite-volume numerical model, with rock types and ranges of allowable values determined by experts, and the discretization taken from previous work. Including a continuum discretization would allow the solution to determine geological features such as rock boundaries or fracture zones. An example of a variable discretization is the continuum triangulation of the plane by Nicholls [10] that we look to include in future analyses.

The posterior distribution $\pi(\theta|\tilde{d})$ given in (1) summarises all knowledge about the measurement process and prior knowledge. Exploratory analyses are often aimed at simply quantifying the nature and range of feasible solutions, and may be performed by simply drawing samples from the posterior distribution, as in this paper. More realistic analyses are aimed at making a decision, such as an investment strategy for long-term power production. Then the ability to make robust decisions within a Bayesian framework is a significant advantage over deterministic approaches.

5. MCMC IMPLEMENTATION

MCMC algorithms draw samples from the posterior distribution by generating a sequence, or 'chain', of solutions that have the ergodic property, i.e. that spends time in each region of parameter space proportional to the posterior probability of that region. Implementation of an MCMC sampling algorithm can be straightforward, particularly when simple Metropolis-Hastings dynamics [11] is employed, as in this paper. However, achieving computational efficiency remains something of an art.

The Metropolis-Hastings algorithm generates a random sequence of parameters (or solutions),

$\theta_1, \theta_2, \theta_3, ..., \theta_N$ with limiting distribution equal to the desired posterior distribution, i.e. $\theta_i \sim \pi(\theta|\tilde{d})$ for large *i*. For most implementations adjacent samples are highly correlated, so θ_i and θ_{i+1} will be very similar, however for large lags, i.e. $j >> i$, the parameters θ_i and θ_j may be viewed as independent samples from the posterior distribution. The sequence also has the Markov property, i.e. the distribution of θ_{i+1} depends only on θ_i, and not the whole history of the chain. Hence the algorithm has an iterative form, as follows:

At step *i*, given state θ_i:

(i) Propose new state θ' from some proposal density $q(\theta'|\theta_i)$

(ii) With probability: $\min\left(1, \frac{q(\theta_i\theta')\pi(\theta'|\tilde{d})}{q(\theta'|\theta_i)\pi(\theta_i|\tilde{d})}\right)$

set $\theta_{i+1} = \theta'$, otherwise set $\theta_{i+1} = \theta_i$.

Mild requirements on the proposal density $q(\theta'|\theta_i)$ ensure that this algorithm converges (in probability) to the desired target distribution. In practice these requirements are easy to satisfy, however some care is required to ensure that the resulting algorithm is sufficiently efficient to generate samples in reasonable time. In this paper we used simple component wise random-walk proposals, tuned for correlations between parameter values.

The main computational cost per iteration is evaluation of the posterior density at the proposed state θ' using:

$$\pi(\theta'|\tilde{d}) = \propto L(\tilde{d}|\theta')\pi_{pr}(\theta')$$

since evaluation of the likelihood function in (5) requires evaluation of the forward map. In this sense, MCMC algorithms are similar to optimisation algorithms in sources of computational cost. Unlike optimisation algorithms, sampling algorithms do not converge to a single state, but rather keep sampling from the posterior density indefinitely. In practice, one runs the MCMC sampler long enough to achieve sufficiently accurate estimates in (3), as determined by the sample variance or other means.

6. WELL DISCHARGE TEST

In order to model the discharge test a single layer radial symmetric grid is used. The well is located in the first block, and then 10 small blocks are used adjacent to the well, followed by 65 blocks with a thickness expansion factor of 1.2.

For each forward simulation the rock properties and the initial state of the system must be specified and then the measured historical mass flows are used to drive the model. The full suite of rock properties includes: porosity, density, permeabilities, thermal conductivity and specific heat. Of these only porosity and permeability have a significant influence on the model results and are the parameters that are varied. The other parameters are assigned typical values and are fixed. Since the model is a homogeneous single layer the porosity and permeability are identical for all the blocks in the model, and permeability has only one component (only in radial direction). For the discharge test considered boiling occurs in the reservoir and thus the choice of relative permeabilities is important. Here the van Genuchten model is used which is determined by four parameters. Of these three (m, S_{lr}, S_{ls}) are allowed to vary while one $(S_{vr} = 0)$ is fixed.

The precise elevation of the feed-zone for the well is not known and therefore the initial temperature (T_0) or saturation (S_{v0}) and initial pressure (p_0) are allowed to vary. Thus the following parameters have to be estimated:

$$\theta = (\phi, \log(k), p_0, T_0 (\text{or } S_{v0}), m, S_{lr}, S_{ls})$$

Here we have transformed permeability to the base 10 logarithmic scale for easier calibration.

6.1 Observed Data

Production rate, flowing enthalpy and well-head pressure were collected during a 140 days period. As shown in Figure 2 the production rate was increased from 4 kg/s to 10 kg/s after day 105.

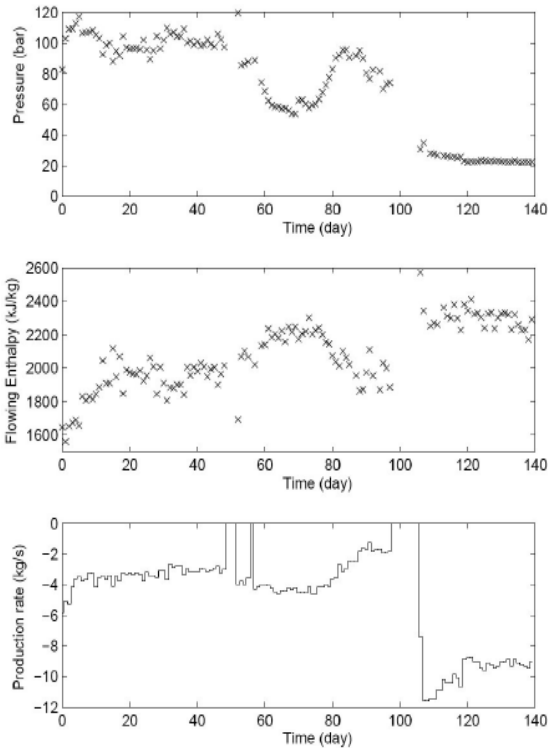

Figure 2. Data collected from the extended discharge test.

This proved to be difficult to deal with in forward simulations as with a low permeability value (k < 1 millidarcy) after day 105 the pressure dropped too low. As shown later in the calibration results, to match the data before day 105, the feasible range of permeability is usually below 1 millidarcy. Further, it is not possible to match the rise in the enthalpy and increase in the pressure while the production rate is falling from day 0 to day 10. Thus in our analysis only the data collected from day 14 to day 84 is used.

Unfortunately, the observed pressures are measured at wellhead whereas the TOUGH2 model generates downhole pressures. Two approaches were used to deal with this problem:
(a) The pressure difference was considered as a constant but unknown parameter p_s
(b) Or it was calculated by using a wellbore simulator for each pressure record ($p_s(t_j)$, j = 1,…,N_W).

The wellbore simulator WELLSIM [12] was run to a steady state to work out the pressure drop for a given configuration of the well, wellhead pressure and flowing enthalpy. The resulting ``steady state'' pressure drop was used as an approximate representation of the transient behaviour.

Note that when the pressure drop is treated as a constant, we have to estimate the pressure shift p_s. Then, the parameter set becomes $\theta' = (\theta, p_s)$. In the top plot of Figure 2, the black and blue crosses are the observed wellhead pressures and the blue crosses are the downhole pressures calculated with the WELLSIM. The wellhead pressure is smoother than the downhole pressure, and because of the lower enthalpy the pressure difference from day 10 to day 55 is larger than the pressure difference from day 55 to day 85.

The data are assumed to satisfy the observation model

$$h_{f;d}^{(t_j)} = h_f^{(t_j)} + \varepsilon_h$$
$$p_{h;d}^{(t_j)} = p_h^{(t_j)} + \varepsilon_p$$

Here ε_h and ε_p are independent and normally distributed measurement errors with zero mean and constant variances σ_h^2 and σ_p^2, respectively. The error standard deviations σ_h = 50 KJ/kg and σ_p = 3 bar were estimated from the residual of a smoothed spline interpolation of the data and from reservoir engineering experience.

6.2 Prior Distribution

The prior probability density for discharge test analysis can be written as a product of the prior probability densities of each individual component of θ and θ':

$$\pi_{pr}(\theta) = \prod_{i=1}^{n} \pi_{pr}(\theta_i)$$
$$\pi_{pr}(\theta') = \pi_{pr}(\theta)\pi_{pr}(p_s) \qquad (5)$$

For the production rate q_m and the relative permeability parameter S_{vr} we use the improper prior distribution $\pi_{pr}(q_m, S_{vr}) \propto 1$, as the production rate is given, and the van Genuchten-Mualem model with $S_{vr} = 0$ was used in this study. Table 1 shows the constraints on the component parameters of θ. Note that the previous study [2] of this discharge test showed that the system is two-phase, and hence we use pressure p and vapour saturation S_v to represent the state of the system. In addition, we choose the following exponential distribution to represent the prior density of each component of θ and θ' (except log(k)):

$$\pi(x) \propto \frac{x}{s}\left(1 - \frac{x}{s}\right)\exp\left(\iota\frac{x}{s}\right)$$

Here s is the factor to scale the parameters into the range (0, 1) and ι is a non-zero constant which control the skewness of the distribution, and sets the high probability region in which the parameter is more likely to occur. Different values of ι are chosen for different components of the parameters θ and θ', as shown in Table 1.

Parameter	Units	Upper Bound	Lower Bound	Skewness
ϕ		1	0	-5

log(k)	[m^2]	-12	-18	-
m		1	0	5
S_{lr}		1	0	2
S_{ls}		1	0	10
p_0	[bar]	250	50	-2
S_{v0}		1	0	-10
p_s	[bar]	150	50	-2

Table 1. The physical bounds for θ and θ'

6.3 Inversion Result

The posterior distribution introduced in (1) is explored by MCMC. The mean value of output is used to estimate the well performance. We use the data from day 14 to day 19 and day 53 to day 69 for training (triangles), and the remaining data is used for validation (squares). Figure 3(a) shows the inversion results for θ and Figure 3(b) shows the results for θ'. The uncertainty in pressure and enthalpy predictions is estimated as ±3 standard deviations of the TOUGH2 outputs of the corresponding random samples (shown as the shaded region).

Both scenarios (with/without the use of the wellbore simulator) are able to produce a reasonable prediction of enthalpy changes.

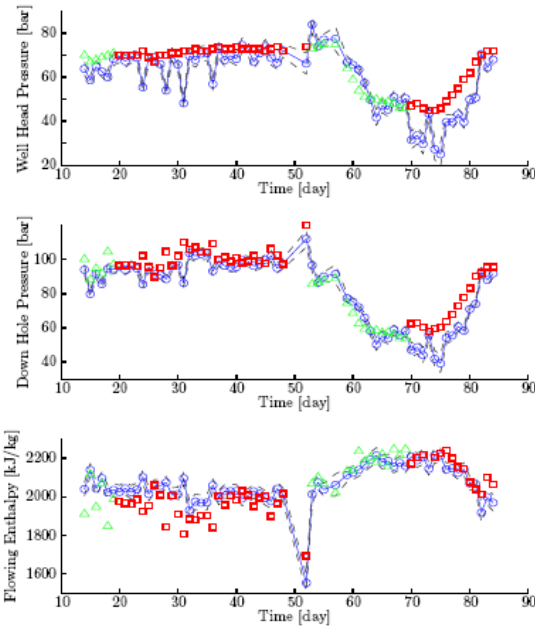

(a)

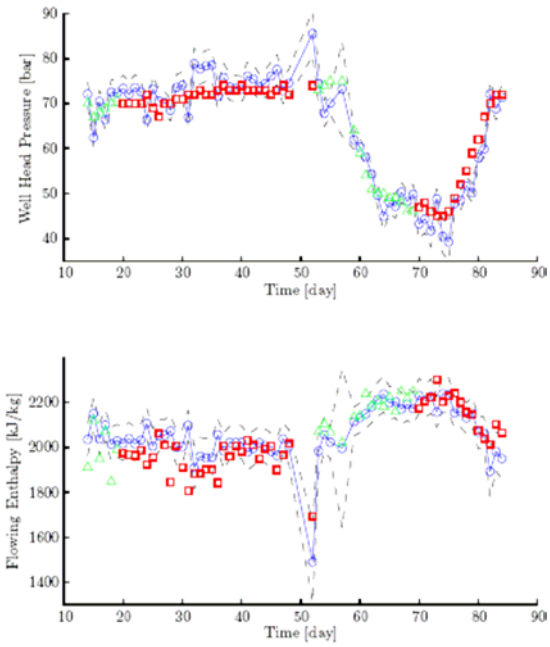

(b)

Figure 3. Predictions of pressure and enthalpy changes. (a) pressure difference between WHP and DHP calculated using WELLSIM (b) Constant pressure difference between WHP and DHP.

With the use of WELLSIM to calculate pressure shifts, the model experiences difficulties in matching the relatively strong pressure drop between day 60 and day 80. In contrast, its peer θ' did a better job during this period, using the constant pressure shift assumption. However compared to the previous work [2] carried out with the optimization package ITOUGH2 our MCMC techniques gives a more accurate and robust result.

In both of the parameter sets θ and θ', we can observe a strong negative correlation between log of permeability (log(k)) and initial pressure (p_0) and also a strong negative correlation between initial vapour saturation (S_{v0}) and the relative permeability parameter S_{ls} (see Figures 4-7).

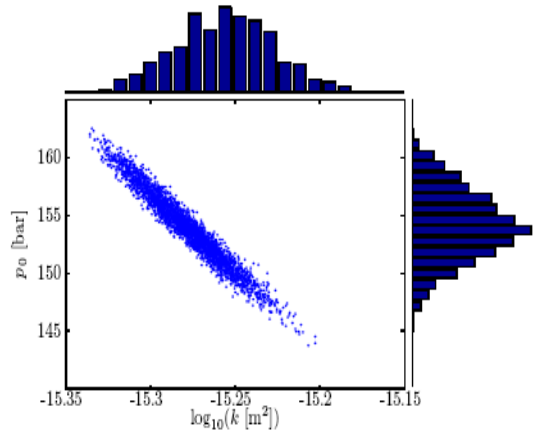

Figure 4. Histograms for the marginal distribution of log(k) and p_0 and a scatter plot of their joint marginal density (pressure difference between WHP and DHP calculated using WELLSIM)

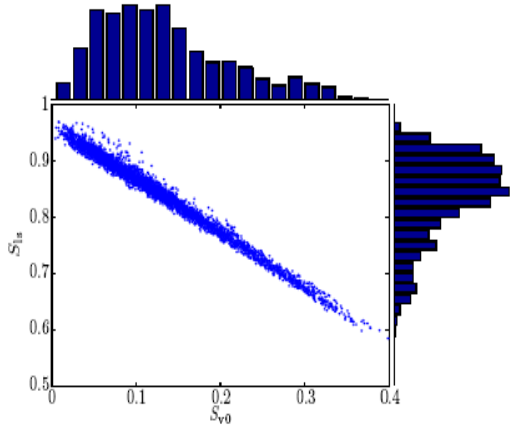

Figure 5. Histograms for the marginal distribution of S_{v0} and S_{ls} and a scatter plot of their joint marginal density (pressure difference between WHP and DHP calculated using WELLSIM)

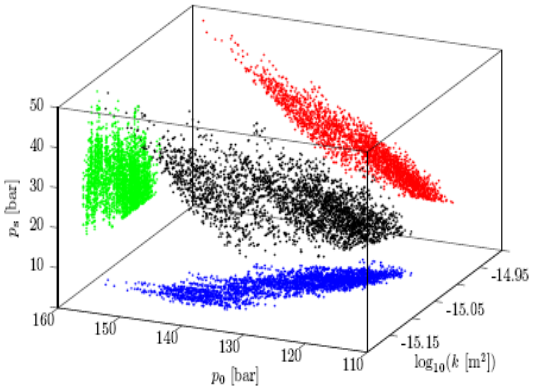

Figure 6. Scatter plot of the joint marginal distribution of log(k), p_0 and p_s (constant pressure difference between WHP and DHP)

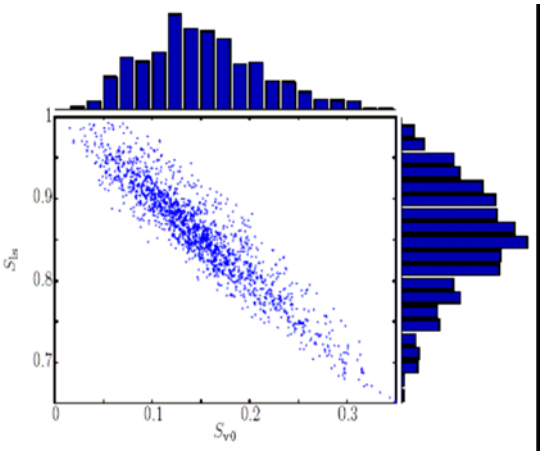

Figure 7. Histograms for the marginal distribution of S_{v0} and S_{ls} and a scatter plot of their joint marginal density (constant pressure difference between WHP and DHP)

7. NATURAL STATE MODEL

The 3-D finite volume grid for the natural state model consists of 7023 blocks. Since most of the wells and therefore most of the temperature measurements (1183 out of 1203) are in the middle of the reservoir, we use a fine grid in this region and a coarse grid in the remaining region.

In natural state modelling problem, since the porosity and initial conditions do not affect the results and the relative permeability function has only a minor impact on the results, they have been removed from the parameter set. Also, we assume the mass and heat input are not variable (this improves the computational efficiency, as varying mass and heat input leads to a long run-time for modelling the natural state). Thus, the parameter set for natural state modelling is:

$$\theta = \left(\underline{k}^i;\ i = 1,\ldots,N\right)$$

There are thirteen temperature profiles measured from different wells. Since the temperature measurements are made on a finer scale than the results from the finite volume TOUGH2 model, we interpolate the TOUGH2 simulated result at each measurement point by bilinear interpolation. The data are assumed to satisfy the observation model

$$T_d^j = T^j + \varepsilon_T^j, \quad j = 1,\ldots,N \qquad (7)$$

With the assumptions we made previously, the error in (7), ε_T^j, represents independent and normally distributed measurement errors with zero mean and constant variance σ_T^2. The error standard deviation σ_T = 3˚C is estimated by calculating the residual of a fitted polynomial for temperature data in each well.

Previously one of the authors (O'Sullivan) calibrated this model manually, and our starting state of MCMC sampling is based on random perturbations to his model. When we perform the MCMC sampling on the unnormalized posterior in equation (1), our current algorithm has difficulties in converging to the target posterior distribution. The maximum likelihood estimate is used instead of the mean estimate, calibration results for some of the wells are shown in Figures 8-14.

In all the plots the red line is the observed temperature profile, the dashed black line is the initial guess, the green line is the results achieved by O'Sullivan using manual calibration and the blue line is our present ML (maximum likelihood) estimate.

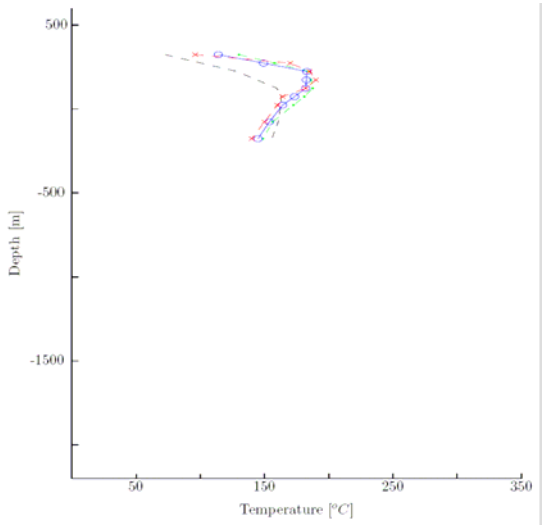

Figure 8. Temperature profile for well A.

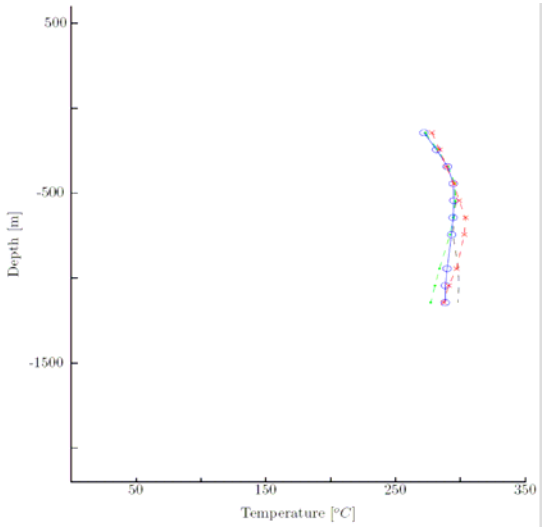

Figure 9. Temperature profile for well B

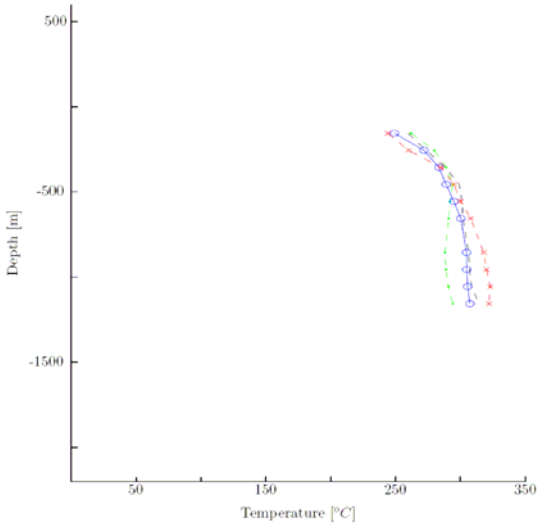

Figure 10. Temperature profile for well C

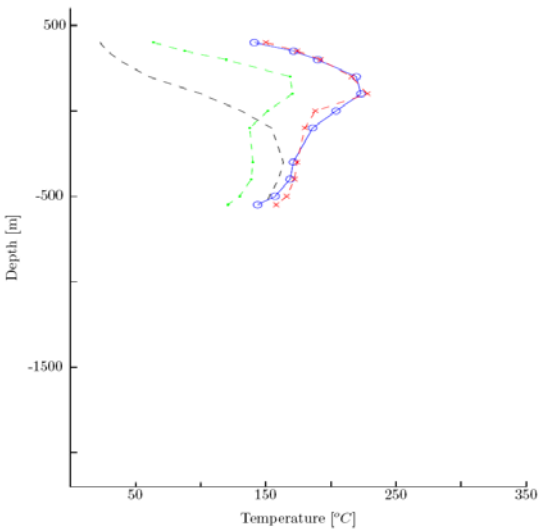

Figure 11. Temperature profile for well D

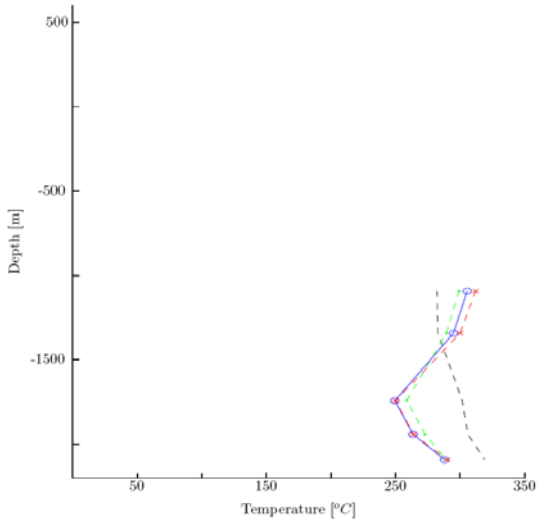

Figure 12. Temperature profile for well E

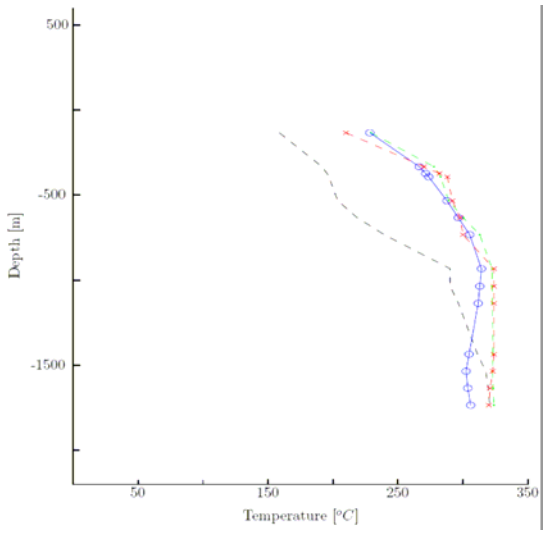

Figure 13. Temperature profile for well F

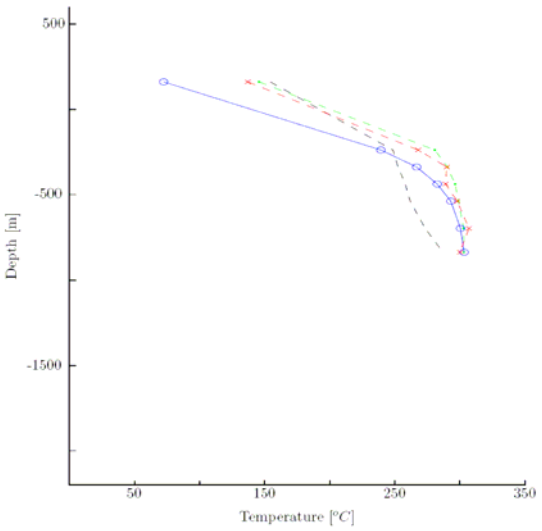

Figure 14. Temperature profile for well G

For well A and some other wells (not shown) our ML estimate produces a match of similar quality the O'Sullivan model. However, the O'Sullivan model performs slightly better for well F and well G. Both our ML estimate and the O'Sullivan model cannot produce close a match to the temperature measurements in well B and well C, but our ML estimate shows a slightly better match. In the well D and well E, our ML estimate gives a better match and the model temperatures are almost identical to the observed temperatures. For the other wells (not shown) our ML estimates give a somewhat better match than the O'Sullivan model.

8. DISCUSSION

The aim of this study was to developing statistical methods to solve the inverse problems for the extended discharge test and the natural state model that automate the calibration process. The results of the two case studies show that our sample based inference for inverse problems provides an efficient and robust calibration approach via MCMC sampling for geothermal models. Compared to a manual approach or a deterministic approach (using iTOUGH2 for example), our approach provides a range of feasible parameters consistent with the observed data through the posterior distribution rather than a single value estimate.

To take the full advantage of sample based inference for geothermal model calibration there are several possible improvements that could be made in the future. For example:
(i) Construct a likelihood function that is able to deal with the spatial-temporal correlation in measure data.
(ii) The temperature profiles shown above are the raw data measured in wells, with no interpretation used. In some cases the presence of internal flows may be disguising the true reservoir temperature. This problem could be overcome by embedding a wellbore simulator into TOUGH2 to handle the internal flow and pressure difference between wellhead pressure and downhole pressure at runtime.
(iii) The vertical grid spacing in our model is too coarse to represent the detailed temperature changes along the well. The model match could be improved by using a sequence of models with each grid a refinement of the previous one, and with the first estimate of parameters for a fine grid obtained by interpolating values form a coarse grid.
(iv) The MCMC process we used assumes that the results obtained from a forward run of TOUGH2 contain no errors. This is not true as discretisation necessarily introduces errors. This problem requires further investigation with statistical techniques that quantify and perhaps utilize modelling errors or bias.

REFERENCES

[1] Finsterle, S. (1993) *ITOUGH2 User's Guide Version 2.2*, Report LBL-34581, Lawrence Berkeley National Laboratory, Berkeley, California.

[2] Finsterle, S., Pruess, K., Bullivant, D.P. and O'Sullivan, M.J. (1997) *Application of inverse modelling to geothermal reservoir simulation*, Proceedings of the 22nd Workshop on Geothermal Reservoir Engineering, Stanford University, Stanford, California, 1997, pp. 309-316.

[3] Hurn, M., Husby, O. and Rue, H., (2003), *Advances in Bayesian image analysis, in Highly Structured Stochastic Systems*, Peter J. Green, Nils Lid Hjort and Sylvia Richardson eds., Oxford Statistical Science Series, 27, Oxford University Press.

[4] Nicholls, G. K. and Fox, C., (1998), *Prior modelling and posterior sampling in impedance imaging*. In Bayesian Inference for Inverse Problems, Proc. SPIE 3459, 116-127.

[5] Vauhkonen, P., Vaukonen, M., Savolainen, T. and Kaipio, J. (1999). *Three-dimensional electrical impedance tomography based on the complete electrode model*. IEEE Trans. Biomed. Eng. 46, 1150-1160.

[6] Kolehmainen, V., Vaukonen, M., Kaipio, J. and Arridge, S.R., (2000). *Recovery of piecewise constant coefficients in optical diffusion tomography, Optics Express*, 7, 468-480.

[7] Kaipio, J. and Somersalo, E. (2004) *Statistical and Computational Inverse Problems*. Springer.

[8] Fox, C., and Nicholls, G.K., (2001), *Exact MAP states and expectations from perfect*

sampling: Greig, Porteous and Seheult revisited. In: Bayesian Inference and Maximum Entropy Methods in Science and Engineering, 20th International Workshop (Gif-sur-Yvette), 8-13 July 2000, edited by Ali Mohammad-Djafari, AIP Conference Proceedings volume 568, 252-263, American Institute of Physics, New York.

[9] Pruess, K., Oldenburg, C. and Moridis, G. (1999) *TOUGH2 User's Guide, Version 2.0*, Report LBNL-43134, Lawrence Berkeley National Laboratory, Berkeley, California.

[10] Nicholls, G.K. (1998) *Bayesian image analysis with Markov chain Monte Carlo and coloured continuum triangulation models*, Journal of the Royal Statistical Society. Series B: Statistical Methodology 60 (3), pp. 643-659

[11] Green, P.J., (1995), *Reversible Jump Markov Chain Monte Carlo Computation and Bayesian Model Determination,* Biometrika, 82(4), 711-732.

[12] Murray, L. and Gunn, C. (1993) *Towards integrating geothermal reservoir and well-bore simulators: TETRAD and WELLSIM*, Proc. 15th New Zealand Geothermal Workshop, pp 279-284.